J. Fluid Mech. (1996), *vol.* 325, *pp.* 399–418

Nonlinear long waves generated by a moving pressure disturbance

By C. M. CASCIOLA[1] AND M. LANDRINI[2]

[1]Dipartimento di Meccanica e Aeronautica, Università di Roma *La Sapienza*, Via Eudossiana 18, 00184 Roma, Italy

[2]INSEAN, Via di Vallerano 139, 00128 Roma, Italy

(Received 23 August 1995 and in revised form 29 January 1996)

The evolution of long waves generated by a pressure disturbance acting on an initially unperturbed free surface in a channel of finite depth is analysed. Both off-critical and transcritical conditions are considered in the context of the fully nonlinear inviscid problem. The solution is achieved by using an accurate boundary integral approach and a time-stepping procedure for the free-surface dynamics.

The discussion emphasizes the comparison between the present results and those provided by both the Boussinesq and the related Korteweg–de Vries model. For small amplitudes of the forcing, the predictions of the asymptotic theories are essentially confirmed. However, for finite intensities of the disturbance, several new features significantly affect the physical results. In particular, the interaction among different wave components, neglected in the Korteweg–de Vries approximation, is crucial in determining the evolution of the wave system. A substantial difference is indeed observed between the solutions of the Korteweg–de Vries equation and those of both the fully nonlinear and the Boussinesq model. For increasing dispersion and fixed nonlinearity the agreement between the Boussinesq and fully nonlinear description is lost, indicating a regime where dispersion becomes dominant.

Consistently with the long-wave modelling, the transcritical regime is characterized by an unsteady flow and a periodic emission of forward-running waves. However, also in this case, quantitative differences are observed between the three models. For larger amplitudes, wave steepening is almost invariably observed as a precursor of the localized breaking commonly detected in the experiments. The process occurs at the crests of either the trailing or the upstream-emitted wave system for Froude numbers slightly sub- and super-critical respectively.

1. Introduction

The properties of waves in water of finite depth, generated by a moving pressure disturbance running on an initially flat free surface, depend on a few parameters of the forcing. In particular the speed and length of the pressure disturbance are crucial and they are selected here to excite wavelengths long with respect to the water depth h. Under such conditions nonlinear effects, measured in terms of the forcing amplitude, are known to have a predominant role. They are especially noticeable in transcritical conditions, when the speed U of the disturbance almost equals the limiting wave celerity $(gh)^{1/2}$. In this case, in fact, the linear model completely breaks

down (Stoker 1957; Akylas 1984) and more refined theories are necessary to describe, even at a qualitative level, the behaviour of the wave system.

When nonlinear effects and dispersion nearly balance, the class of Boussinesq models is obtained in the limit of small amplitude. In this framework, since Wu developed a generalized Boussinesq (gB) approach for forced systems, the flow generated by a moving pressure patch has been thoroughly analysed. In particular, it was numerically shown by Wu & Wu (1982) that, when $Fr = U/(gh)^{1/2} \simeq 1$, a periodic emission of upstream-running wave packets occurs and, though the forcing is time independent, the flow is not able to attain a steady state. Akylas (1984) and Cole (1985), starting from the blow-up of the critical linear solution, achieved the same phenomenon and showed that, far from the forcing, the wave motion obeys a singularly forced Korteweg–de Vries (KdV) equation. Forced KdV equations have also been used by Melville & Helfrich (1987) to model transcritical conditions in stratified flows and eventually extended to the three-dimensional problem (Tomasson & Melville 1991). In this context the major difference from the corresponding free-surface problem is a cubic nonlinearity which substantially modifies the nature of the transcritical regime.

Weakly nonlinear formulations also provide an effective model for off-critical conditions when the forcing is designed to generate long waves. Specifically, Kevorkian & Yu (1989) by means of a multiple-scale approach devised approximate solutions of the Boussinesq system described in terms of three uncoupled waves. Two of them are governed by homogeneous KdV equations in which the initial conditions depend on the 'shape' and the speed of the forcing. The third wave is stationary with respect to the pressure disturbance.

In experiments, the emission of runaway soliton–like pulses in transcritical flows was observed in towing tank tests by Thews & Landweber (1936); while, operating in a similar context, Huang *et al.* (1982) later rediscovered the same phenomenon (see also Ertekin, Webster & Wehausen 1984). Successively, specially designed experiments, with the disturbance originated by a suitably moving bottom topography, broadly confirmed the approximate theory for transcritical flows (Lee, Yates & Wu 1989). It may be noted however, that unavoidable uncertainties hamper the comparison between theory and experiments; in particular some difficulties in detecting incipient wave breaking are encountered and the effects on the waves of the boundary layer at the moving topography are difficult to assess quantitatively.

These considerations suggest comparison of the weakly nonlinear theories with accurate numerical solutions of the nonlinear inviscid problem in an attempt to point out the possible relevance of the terms neglected in the approximate approaches. For this purpose, we consider fully nonlinear solutions together with the predictions of two basic formulations: namely the generalized Boussinesq model and the related Korteweg–de Vries description. The latter approach, in particular, exhibits several nice features that we would like to exploit. Despite the possibly larger degree of approximation, it gives a more direct insight into the mechanics of forced long waves. Moreover it predicts a sort of amplitude invariance when properly scaled variables are chosen. A rational guideline may follow for discussing the present nonlinear results. However, since the scaling does not hold exactly for the original Boussinesq model, it is convenient to consider numerical solutions of both the approximate formulations.

In this context, a large set of numerical solutions of the nonlinear problem are carefully discussed. In particular, the effect of increasing pressure amplitudes is analysed in detail. As expected, the scaling suggested by the KdV approximation is recovered in the small-amplitude limit. Nevertheless, discrepancies are observed for small finite intensities of the forcing. Their origin is discussed at length. For off-critical flows, we

suggest the interaction among the different components of the wave pattern, occurring during the initial stage, as the mechanism which explains the differences observed between the KdV solutions and the present exact calculations. This conjecture is substantiated by solving the Boussinesq problem, where the interactions, intrinsic to this model, yield results almost exactly matching the nonlinear computations. With regard to the critical regime, for increasing amplitude of the forcing, more marked differences are observed between the Boussinesq approximation and the numerical solutions of the exact problem.

Although a systematic analysis in this direction has not been undertaken, incipient wave breaking is often observed in the numerical experiments, an aspect considered in more detail by Teles da Silva & Peregrine (1992) for the case of a moving bottom topography. Actually, a complete theory of breaking is not at present available, but it is known, Dommermuth *et al.* (1988), that fully nonlinear inviscid calculations may provide an accurate description of the steepening phase, immediately preceding the actual wave breaking. In fact, our results qualitatively reproduce the corresponding experimental observations (Lee *et al.* 1989; Ertekin *et al.* 1984). Namely, for transcritical flows at a fixed amplitude of the forcing, when the subcritical detuning from $Fr = 1$ is increased, the trailing crest is always observed to undergo a localized steepening. For increasing supercritical detuning, we find the first forward running wave manifesting a definite tendency towards overturning.

The numerical formulation of the nonlinear problem is essentially based on a boundary integral representation for the velocity field, Casciola & Piva (1990), and a stepping procedure for the free-surface evolution, Longuet-Higgins & Cokelet (1976). As a whole, the algorithm is similar to others previously used to simulate unsteady free-surface flows (see e.g. Vinje & Brevig 1981; New, McIver & Peregrine 1985; Baker, Meiron & Orszag 1989). Details are discussed in §2. Since the present work has been essentially conceived as a comparison between the fully nonlinear description and basic weakly nonlinear models, in §3 the relevant theoretical results are recalled, essentially with the aim of introducing the scalings extensively used in the following. This section, where no particularly new result is introduced, is in fact a review based on the multiple-scale formalism as originally proposed in Kevorkian & Yu (1989). Sections 4 and 5 describe the forced wave patterns for off-critical and transcritical flows respectively and, finally, some conclusions are drawn in §6.

2. The fully nonlinear approach

In a channel of uniform depth h, a motionless fluid of density ρ subject to gravity, g, is considered. The vertical direction defines the y-axis with unit vector $\boldsymbol{j}$ pointing upwards. At time $t^\star = 0$ a pressure disturbance $p^\star$, with compact support of length 2ℓ, suddenly forces the initially flat free surface. The pressure excitation moves, with respect to the undisturbed fluid, in the negative x-direction at constant velocity U and generates an irrotational wave system. For wavelengths long compared with the depth, a velocity scale is suitably determined by the linear limiting speed $\mathscr{C}_0 = (gh)^{1/2}$, which fixes the relevant Froude number as $F = U/\mathscr{C}_0$. The two other quantities required to recast the problem in dimensionless form are chosen as the constant density ρ and as the initial depth h respectively. Accordingly the dimensionless pressure is $\mathscr{P} = p^\star/(\rho g h)$.

A sketch of the geometry and the corresponding nomenclature are given in figure 1. The wave profile $\mathscr{F}$, with unit tangent and normal vectors τ and ν respectively, is

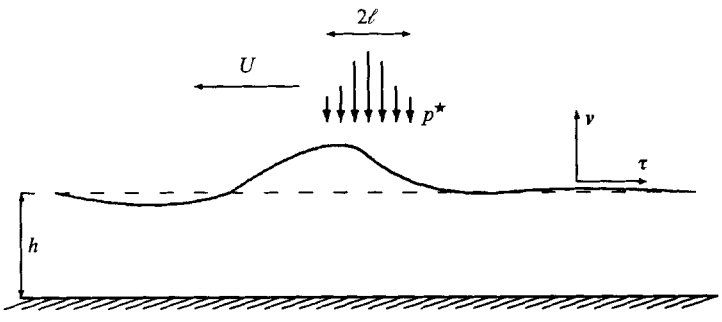

FIGURE 1. Geometry of the problem and nomenclature adopted.

described by the parametric equations

$$x = x(\alpha, t), \qquad y = y(\alpha, t), \qquad \alpha \in \mathscr{I}_\alpha , \tag{2.1}$$

where α is a curvilinear coordinate along the free surface. By exploiting the material nature of the interface, α may be identified with a Lagrangian parameter along $\mathscr{F}$. Hence the kinematic condition is simply

$$\frac{\mathrm{D}\boldsymbol{x}}{\mathrm{D}t} = \boldsymbol{v} , \tag{2.2}$$

with $\boldsymbol{v} = \boldsymbol{u} - \boldsymbol{U}$ the velocity in the frame of the disturbance and $\boldsymbol{u}$ the perturbation of the free stream $-\boldsymbol{U}$. The tangential projection of the incompressible Euler equation yields the dynamic condition in the form

$$\frac{\mathrm{D}u_\tau}{\mathrm{D}t} = u_v \boldsymbol{v} \cdot \frac{\mathrm{D}\boldsymbol{\tau}}{\mathrm{D}t} - \frac{\partial \mathscr{P}}{\partial \tau} - \boldsymbol{j} \cdot \boldsymbol{\tau} , \tag{2.3}$$

which holds in the general rotational case (Casciola & Piva 1990). After introducing the tangent vector $\boldsymbol{e}_\alpha = (\partial x/\partial\alpha, \partial y/\partial\alpha)$, a more compact expression,

$$\frac{\mathrm{D}u_\alpha}{\mathrm{D}t} = \frac{\partial}{\partial \alpha}(\tfrac{1}{2}u^2 - \eta - \mathscr{P}) , \tag{2.4}$$

is achieved in terms of the covariant velocity component $u_\alpha = \boldsymbol{u} \cdot \boldsymbol{e}_\alpha$.

The velocity field in the fluid domain may be expressed in terms of the Poincaré representation formula, Bassanini *et al.* (1991), which for irrotational flows, after introducing the unit vector $\boldsymbol{k}$ normal to the flow plane, reads

$$\boldsymbol{u}(\boldsymbol{x}^\star) = -\nabla^\star \int_{\mathscr{F}} u_v G^+ \,\mathrm{d}\ell + \nabla^\star \times \int_{\mathscr{F}} u_\tau \boldsymbol{k} G^- \,\mathrm{d}\ell , \tag{2.5}$$

where the boundary condition $\boldsymbol{u} \cdot \boldsymbol{v} = 0$ at the bottom of the channel has been implicitly enforced through the method of images. In particular, by denoting with a subscript s the mirror image of a point with respect to the bottom, the kernel functions in (2.5) are

$$G^\pm = \frac{1}{2\pi}\left(\ln|\boldsymbol{x} - \boldsymbol{x}^\star| \pm \ln|\boldsymbol{x}_s - \boldsymbol{x}^\star|\right) .$$

An integral equation for u_v may be obtained from (2.5) by projecting along the normal $\boldsymbol{v}$, after considering the limiting form of the integral representation as the point $\boldsymbol{x}^\star$ approaches the free surface. The system consisting of the boundary integral equation, coupled with (2.2), (2.4), describes the nonlinear dynamics of the unsteady

free surface. An approximate solution may be obtained by means of a stepping procedure, where a standard fourth-order Runge–Kutta scheme is used to solve the evolution equations (2.2), (2.4). At each sub-step a boundary integral equation is solved to determine u_ν from the configuration of the free surface and from the values of u_τ. The integral equation is approximated via a quadrature method (Cooker *et al.* 1990) based on the Euler–MacLaurin summation formula, see e.g. Sidi & Israeli (1988). By this method spectral accuracy is normally achieved for compactly supported densities, as they may be assumed, on physical grounds, for finite times after the onset of the pressure disturbance. However, since we aim to analyse long evolutions, we are forced to truncate the computational domain. In these conditions, u_τ and u_ν as well as the free-surface elevation do not vanish at the edges and unphysical reflections usually occur. This drawback is avoided by the introduction of artificial damping layers (Israeli & Orszag 1981; Baker *et al.* 1989), which, by forcing the densities to vanish towards the edges of the computational domain, prevent the unwanted reflections. In principle this procedure may reduce the accuracy of the computation, which however is maintained under control by performing an *a posteriori* check, i.e. by comparing different solutions for increasing domain lengths. In particular, the evolution equations (2.2), (2.4) are modified according to

$$\frac{\mathrm{D}\boldsymbol{x}}{\mathrm{D}t} = \boldsymbol{v} - \mu\eta\,\boldsymbol{j}, \qquad \frac{\mathrm{D}u_\alpha}{\mathrm{D}t} = \frac{\partial}{\partial\alpha}(\tfrac{1}{2}u^2 - \eta - \mathscr{P}) - \mu u_\alpha\,. \tag{2.6}$$

The damping coefficient, $\mu(x)$, is zero everywhere except within the damping regions, where it increases quadratically from zero to a suitable value μ_{max} attained at the outer edge of the sponge layer. The length ℓ_d of the two damping layers and the maximum damping coefficient, μ_{max}, have been heuristically determined and typical values are $\ell_d/\ell \simeq 2$ and $\mu_{max}\,h/\mathscr{C}_0 \simeq 0.5$ respectively.

The quadrature formula chosen to discretize the boundary integral equation requires the derivative of the tangential velocity as well as the wave slope and curvature. Hence the accuracy of the computation strongly depends upon the discrete representation adopted for the densities and the geometry. In particular both Fourier (Roberts 1983) and Lagrange polynomials (Dold 1992) have been tested, using standard FFT techniques in the former case. No significant difference between the two approaches has been detected so far and, since a slightly more efficient code results, the actual algorithm relies upon the fully spectral approach. To enhance the computational performances, an iterative solver is used instead of a direct matrix inversion.

For the present scheme, a sawtooth instability, originally discussed by Longuet-Higgins & Cokelet (1976), usually sets in for long evolutions. It is found to be almost independent of the time step chosen, and tests with Stokes waves indicate that it is related to the steepness, i.e. the breakdown time is anticipated for steeper waves. To remove the instability high-order filtering procedures (see Dold 1992) are used, after verifying the conservation of several invariants of motion.

In terms of computational efficiency, the resulting code requires the evaluation of four influence matrices per time step and the solution of the corresponding algebraic systems, which however is rapidly obtained by means of an iterative solver. A significant speed up could be achieved by a different stepping procedure, based on the analytical continuation in time of the solution (Dold & Peregrine 1986). The resulting algorithm also presents better stability characteristics and reduces the need for the smoothing of the solutions. However, since the physical results are not significantly altered by the filtering, the present approach was selected for its simpler implementation. A further point we would like to mention, although not directly

concerned with the present problem, is the easier extension to rotational flows in the context of vortex methods.

All the results presented, obtained on a IBM RISC 6000 mod. 540 workstation, have been checked under spatial and temporal refinement. In particular, each run has been repeated with finer parameters until a convergence within four significant digits of the L^2 norm is achieved for the final configuration of the free-surface elevation. Typically, the number of nodes on the free surface ranges from 512 to 2048 while up to 10000 time steps are required for the longest evolutions considered.

3. Weakly nonlinear theory

When the pressure disturbance and its speed U are selected to generate long waves of small amplitude, the problem formulated in the previous section can be conveniently modelled in terms of weakly nonlinear–weakly dispersive theories. We present here a brief account of those theoretical aspects we have found useful in discussing the results of the fully nonlinear calculations. In particular, we consider the generalized Boussinesq model and the ensuing KdV formulation.

In the long-wave limit two different lengths characterize the problem, namely an horizontal scale L, related to a typical wavelength, and a vertical scale h, the undisturbed channel depth. The strength of nonlinear effects is estimated by the ratio $\epsilon = a/h$ of a typical wave amplitude to water depth, which, in the weakly nonlinear limit, is assumed to be a vanishingly small quantity. The amount of dispersion is controlled by the ratio $\delta_L = (h/L)^2$, again a small quantity for weakly dispersive conditions. When δ_L is of the same order as ϵ, one obtains the weakly nonlinear–weakly dispersive regime. In general, as a further parameter given by the Froude number, we have to specify the speed of the disturbance in terms of the long-wave limiting speed $\mathscr{C}_0$. With an appropriate choice of the dimensionless variables,

$$x = \frac{x^*}{L}, \qquad y = \frac{y^*}{h}, \qquad t = \frac{t^*}{L/\mathscr{C}_0}, \qquad \eta = \frac{\eta^*}{\epsilon h}, \qquad u = \frac{u^*}{\epsilon \mathscr{C}_0}, \qquad \mathscr{P} = \frac{p^*}{\rho g h}\ , \tag{3.1}$$

the evolution equations for the waves generated by the disturbance may be reduced to the generalized Boussinesq system

$$\left.\begin{aligned} &\eta_t + F\eta_x + \mathscr{U}_x + \epsilon(\mathscr{U}\eta)_x = 0, \\ &\mathscr{U}_t + F\mathscr{U}_x + \eta_x + \epsilon\mathscr{U}\mathscr{U}_x - \tfrac{1}{3}\delta_L \mathscr{U}_{xxt} - \tfrac{1}{3}F\delta_L \mathscr{U}_{xxx} = -\mathscr{P}_x/\epsilon\ , \end{aligned}\right\} \tag{3.2}$$

where $\mathscr{U}$ denotes the dimensionless depth-averaged value of the horizontal velocity u. A detailed derivation and discussion of (3.2), may be found, among others, in the papers by Wu & Wu (1982), Wu (1987), Lee *et al.* (1989), by Kevorkian & Yu (1989) as well as in the textbook by Mei (1989). We may note that a bounded solution of the above system requires an $O(\epsilon)$ forcing at most, thus suggesting arranging the pressure in the form of an ϵ-expansion

$$\mathscr{P} = \epsilon \Pi_1 \mathscr{P}_1 + \epsilon^2 \Pi_2 \mathscr{P}_2\ , \tag{3.3}$$

where, when dealing with distributions with non-zero spatial average, $\mathscr{P}_1$ and $\mathscr{P}_2$ are conveniently normalized to form a unit integral.

In the generalized Boussinesq system (3.2) the amplitude ratio ϵ appears both explicitly and through the dispersion parameter δ_L. In particular, without any

additional restriction, we set $\delta_L = \epsilon$ which defines the horizontal scale as

$$L = h\epsilon^{-1/2} . \tag{3.4}$$

Consistently we may expect the solution of system (3.2) to depend on ϵ, i.e. essentially on the intensity of forcing. The system has been solved numerically in Wu & Wu (1982) by means of a finite difference scheme. For the purpose of comparison with the fully nonlinear calculations, we choose here the improved algorithm suggested by Wei *et al.* (1995) in their study on higher-order Boussinesq models.

3.1. *The Korteweg–de Vries model*

A more direct insight into the behaviour of the waves may be gained by reducing (3.2) to suitable Korteweg–de Vries equations. To this end, in Kevorkian & Yu (1989) a multiple-scale formalism has been devised by introducing a slow time variable

$$\tau = \epsilon t \tag{3.5}$$

and the related ϵ-expansions for the unknowns

$$\eta = \eta_1(t;\tau;x) + \epsilon\,\eta_2(t;\tau;x), \qquad \mathscr{U} = \mathscr{U}_1(t;\tau;x) + \epsilon\,\mathscr{U}_2(t;\tau;x). \tag{3.6}$$

Consistently the solution at order ϵ is found in the form of two decoupled waves, f and g respectively, which are solutions of two KdV equations,

$$f_\tau + \tfrac{3}{2} f f_\xi + \tfrac{1}{6} f_{\xi\xi\xi} = 0, \qquad g_\tau - \tfrac{3}{2} g g_\zeta - \tfrac{1}{6} g_{\zeta\zeta\zeta} = 0 , \tag{3.7}$$

with initial conditions given by

$$f(\xi, \tau = 0) = \tfrac{1}{2}\Pi_1 \frac{\mathscr{P}_1}{F+1}, \qquad g(\zeta, \tau = 0) = -\tfrac{1}{2}\Pi_1 \frac{\mathscr{P}_1}{F-1}. \tag{3.8}$$

In the above equations, in addition to the slow time τ, the independent variables are the characteristics of the linearized problem,

$$\xi = x - (F+1)t, \qquad \zeta = x - (F-1)t. \tag{3.9}$$

The free-surface elevation is finally recovered as

$$\eta = \Pi_1 \frac{\mathscr{P}_1}{F^2 - 1} + f + g . \tag{3.10}$$

This solution holds when the Froude number is significantly different from one, to avoid the blow-up implied by the initial conditions (3.8). Furthermore the pressure distribution, which gives the initial conditions for the two f- and g-waves, is constrained by the long-wave assumptions, i.e. appreciable variations are required to take place on the long spatial scale L. With the above requirements, the wave system is described, in the reference frame of the disturbance, in terms of a steady component and two signals, namely the f-wave, always right propagating, and the g-wave, either left or right propagating for $F < 1$ and $F > 1$ respectively.

In transcritical flows, a different procedure is required. The blow-up can only be avoided for $\Pi_1 = 0$, i.e. for an order-ϵ^2 pressure forcing. In this case an $O(\epsilon)$ detuning from critical conditions may be consistently considered,

$$F = 1 + \epsilon\lambda, \qquad \lambda = O(1) , \tag{3.11}$$

and the wave system is now entirely defined, at the specified order, in terms of a single g-wave following from a forced KdV equation,

$$g_\tau + \lambda g_x - \tfrac{3}{2} g g_x - \tfrac{1}{6} g_{xxx} = \tfrac{1}{2}\Pi_2 \mathscr{P}_{2x} , \tag{3.12}$$

with homogeneous initial conditions. The proper order of magnitude for the solution requires $\Pi_2 = O(1)$ and even highly compact forcings, in the form of a Dirac distribution on the scale L, are allowed (Akylas 1984). Finally, we mention that the numerical solutions of (3.12) we use in the discussion of the transcritical problem have been computed with the scheme described in Kevorkian & Yu (1989).

3.2. *The pressure distribution*

The amplitude ratio ϵ may be related to known characteristics of the forcing. In particular, we assume, for the sake of simplicity,

$$p^\star = p^\star(x^\star)\,\mathrm{H}(t^\star)\,,$$

where $\mathrm{H}(t^\star)$ is the Heaviside step function, and, consistent with the outlined theory, we set

$$\mathscr{P} = \epsilon\Pi_1\mathscr{P}_1, \qquad\qquad \mathscr{P} = \epsilon^2\Pi_2\mathscr{P}_2 \tag{3.13}$$

for off-critical and transcritical flows, respectively. After defining the pressure force intensity

$$\epsilon_p = \frac{1}{\rho g h^2}\int p^\star \mathrm{d}x^\star\,, \tag{3.14}$$

the above equations relate the amplitude ratio ϵ to the actual forcing. Namely, $\epsilon_p = O(\epsilon^{1/\alpha_i})$ where $\alpha_1 = 2$ and $\alpha_2 = 2/3$ are the appropriate exponents for the off-critical ($i = 1$) and the transcritical ($i = 2$) case, respectively. Without loss of generality, we may enforce $\epsilon_p = \epsilon^{1/\alpha_i}$ to yield, in the two cases, $\Pi_1 = 1$ and $\Pi_2 = 1$. This relates the horizontal length scale to the forcing intensity, $L = h\epsilon_p^{-\alpha_i/2}$, and determines the distributions

$$\mathscr{P}_i = \frac{p^\star}{\rho g h \epsilon_p^{i\alpha_i}}\,, \qquad i = 1,2\,, \tag{3.15}$$

defined by the two equations (3.13). Finally, according to (3.1),(3.4) and the connection between ϵ and ϵ_p, $x = x^\star/(h\epsilon_p^{-\alpha_i/2})$.

With these scalings, we see that either the initial conditions (3.8) for the homogeneous KdV equations (3.7) in off-critical flows, or the forcing term of equation (3.12) for the transcritical case, are entirely determined by the corresponding shape function $\mathscr{P}_i(x)$. Namely, these functions define an equivalence class of forcings which yield ϵ_p-independent solutions for the relevant KdV equations. Within each class, any element is determined by its pressure force intensity ϵ_p which, given the channel depth h, fixes the scaling between x and $x^\star$ and, through equation (3.15), the pressure distribution $p^\star$ in physical variables. In most of the cases considered, the physical pressure acting upon the initially undisturbed free surface is obtained from the compactly supported distribution

$$\mathscr{P}_i(x) = \begin{cases} \tfrac{1}{2}K(\,1 + \cos(\pi K x)\,), & |x| < 1/K, \\ 0, & |x| > 1/K, \end{cases} \qquad i = 1,2\,. \tag{3.16}$$

4. Sub- and super-critical conditions

Here results, as obtained by the nonlinear modelling of §2, are contrasted with the predictions of the weakly nonlinear theory summarized in the previous section.

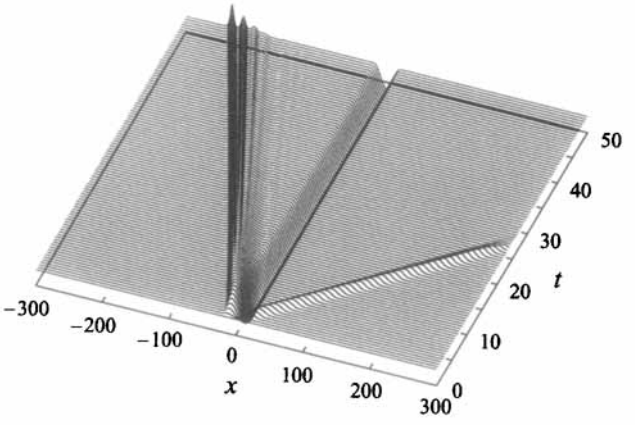

FIGURE 2. Evolution of the free surface in the subcritical case ($F = 0.5$, $K = 0.025$, $\epsilon_p = 2.0$). The horizontal coordinate x and the wave elevation are scaled with the initial depth h and $t = t^* C_0/h$.

The physical pressure distribution, corresponding to (3.16), has a compact support of length $2\ell = 2h/(K\,\epsilon_p)$ and is readily obtained as

$$p^*(x^*) = \rho\, g\, h\, \epsilon_p^2\, \mathscr{P}_1(\epsilon_p\, x^*/h). \tag{4.1}$$

It may be noted that the parameter K appearing in (3.16) is the ratio L/ℓ of the characteristic horizontal scale to half the support length.

Even in the context of the KdV ϵ_p-independent approximation, the solution in physical variables presents an involved dependence on the intensity of the forcing, owing to the relative motion of the three wave components which spread out on the fast time scale, while nonlinearly self-interacting on the slower one. This circumstance, which may hamper the assessment of genuine nonlinear effects, is easily bypassed by analysing the present results in terms of the variables

$$\xi = \epsilon_p \left(\frac{x^*}{h} - (F+1)\frac{t^*}{h/\mathscr{C}_0} \right), \qquad \zeta = \epsilon_p \left(\frac{x^*}{h} - (F-1)\frac{t^*}{h/\mathscr{C}_0} \right),$$

$$\tau = \epsilon_p^3 \frac{t^*}{h/\mathscr{C}_0}, \qquad \eta = \frac{\eta^*}{h\epsilon_p^2}$$

suggested by the multiple-scale formalism. In this description we expect, at leading order, the different wave components to exhibit the ϵ_p-independence, appropriate to the KdV model, and we are allowed to ascribe any different behaviour to the neglected nonlinearities.

4.1. *Subcritical regime*

In the following we assume $h = 1.0$ and, unless otherwise stated, $K = 0.025$. A typical evolution of the free surface in the reference frame of the external pressure field is described in figure 2. A steady depression develops under the disturbance, centred around $x = 0$, which, in the frame of the undisturbed fluid, moves in the negative x-direction. The two unsteady components correspond to the f- and g-waves considered in §3.

With the adoption of the slow time τ and the characteristic variable ζ to follow the g-wave, several cases are considered at $\tau = 1600$ for increasing ϵ_p (figure 3), after veri-

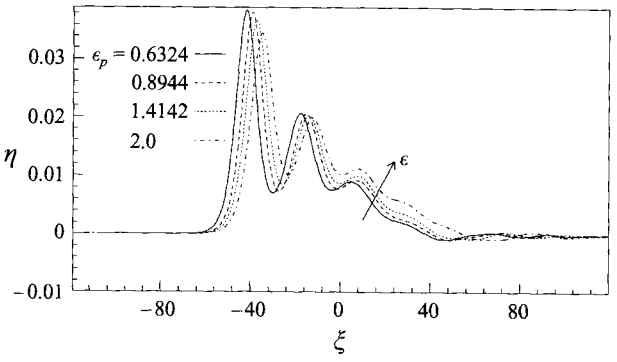

FIGURE 3. Subcritical wave patterns for increasing pressure intensity ϵ_p ($F = 0.5$, $K = 0.025$, $\tau = 1600$).

fying the grid-independence of the solutions. In substantial agreement with the theory for the KdV equation, Segur (1973), the self-interaction of the packets asymptotically leads to a train of solitary waves, in order of amplitude. However, higher-order effects emerge from the comparison of the wave profiles. On the ground of the KdV theory of §3, the physical amplitudes of the emitted packets are expected to linearly increase with ϵ, thus resulting in constant heights in the present dimensionless diagrams. The numerical solutions, instead, clearly indicate a deviation from the theoretical predictions: the physical wave heights are observed to increase less than theoretically expected. This finite-amplitude effect will be further discussed below. Note the phase shift apparent in figure 3, where the stronger packets are delayed with respect to the weaker ones. The origin of this shift is twofold. First, as is known, solitary waves exhibit amplitude dispersion and, to first order, the phase velocity increases linearly with the wave amplitude. This correction is implicitly included in the definitions of τ and ζ. Hence, in the present variables, all curves should collapse one on the other if the first-order correction to the propagation speed were the only one effectively present. Higher-order theories, Fenton (1972), show that the successive terms are always reducing the first-order prediction. Therefore, in this representation, consistently with the present observation, weaker trains (smaller ϵ) should precede stronger ones. Second, due to the described finite-amplitude effect, the strongest waves have, in this case, physical amplitudes reduced with respect to the theoretical KdV predictions. Here amplitude dispersion enters at first order, producing a further reduction in speed. These two aspects combine in determining the observed phase shift. In particular, since the finite-amplitude effect acts at a linear level, it introduces a more effective speed reduction. We thus conjecture the second mechanism to be the predominant one in causing the total phase shift.

The present results suggest in particular the initial transient as the possible origin of the observed behaviour of the packets. This phase is entirely missed by the KdV description, which establishes an equivalence between the complete forced problem, where the pressure perturbs an initially undisturbed free surface, and the free evolution of suitably defined initial data, (3.8). On physical grounds, this results in neglecting the interactions among the (left and right) propagating packets and with the localized depression underneath the external surface forcing. These interactions may become, in principle, more significant for increasing amplitudes of the forcing. In an attempt to quantify their role, we compare the solutions of two different problems: the physical one, where the external pressure generates the wave motion, and a *non-interacting* solution, where the left- and right-propagating packets spread out from an initial

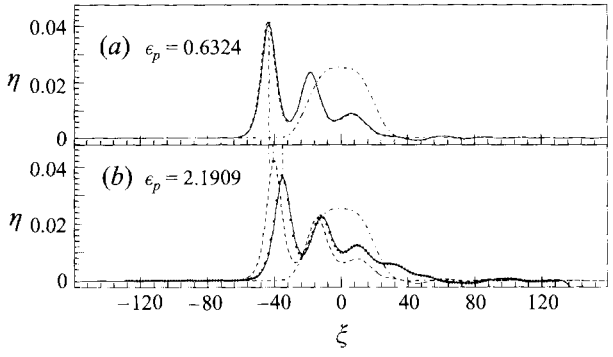

FIGURE 4. Free-surface configurations ($F = 0.5$, $K = 0.025$, $\tau = 1600$) for the complete (solid line) and the non-interacting initial value problems (broken line) for two different forcing intensities. The bump (– · –) represents the initial elevation for the non-interacting solution. The vertical lines are drawn to help estimating the phase shifts. For $\epsilon_p = 2.1909$ (*b*), the solution of the gB equations (•) can hardly be distinguished from the corresponding nonlinear result.

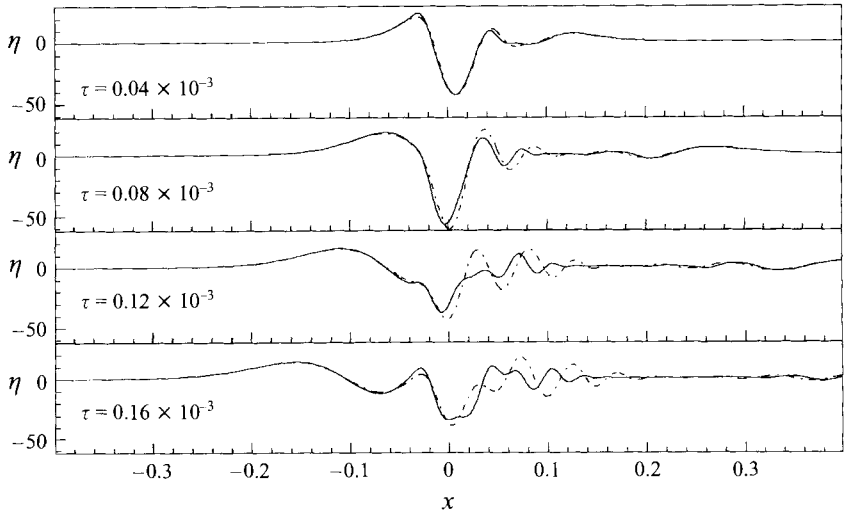

FIGURE 5. The wave pattern ($F = 0.5$, $\epsilon_p = 0.6324$) predicted by the Boussinesq system (dash–dotted line) is compared with the fully nonlinear solution (solid line) for the case of a short support, $K = 25$, of the pressure distribution.

hump shaped according to (3.8) (non-interacting initial value problem). Any observed difference may reasonably be ascribed to the neglected interactions. More precisely, only slight differences are expected for weak forcings, the actual range described by the KdV equation, while the discrepancies should become conspicuous for larger excitation amplitudes. In fact, considering for definiteness only the left-propagating packet, in figure 4 identical evolutions are found for the complete and the non-interacting problems, when the forcing is weak (*a*). When the intensity of the forcing is increased (figure 4*b*), the solutions are apparently different, thus confirming that for larger nonlinearities the mutual interactions among the components of the wave system cannot be consistently ignored.

The different evolutions allow us to assess the relative importance of the two mechanisms explaining the phase shift. Actually, the packets evolving from the

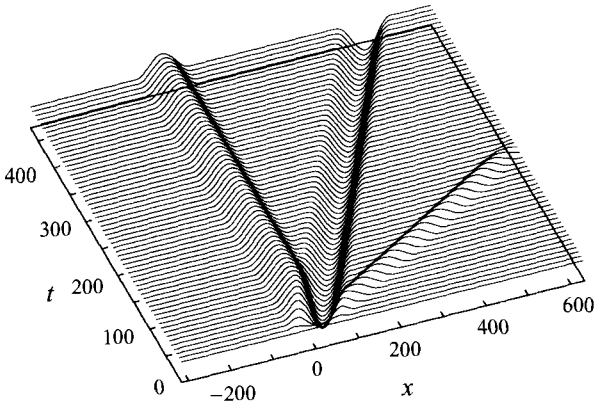

FIGURE 6. Evolution of the free surface in the supercritical case $F = 2.0$. $\epsilon_p = 0.6324$, $K = 0.025$. Variables defined as in figure 2.

initial conditions are, for the larger ϵ_p, slightly delayed with respect to weaker ones (the phase shift between the dashed curves, the first on figure 4(*a*) the second on 4(*b*)). The reduction in speed associated with the finite-amplitude effect is strongly predominant over the other (figure 4*b*), thus confirming the initial conjecture. Since the present results essentially identify the phenomenon with a mutual interaction among different wave components, we may expect the Boussinesq model (3.2) to reproduce the nonlinear wave forms (see the gB solution in figure 4).

The evolution of the right-propagating wave essentially parallels that just described for the left-going system, the main differences being largely explained through (3.8), where the large denominator accounts for the smaller amplitude.

The value of the parameter K, held fixed in the cases just considered, is relatively small. For fixed intensity ϵ_p and shape function, the dispersion effects increase with K (i.e. with reducing the base length) and an intense dispersive tail associated with the wave going left is observed for $K = 25$. For this case, figure 5 compares the free-surface configurations provided by the gB equations (dash–dotted lines) with the nonlinear results (solid lines). The high dispersion is poorly modelled by the standard Boussinesq approximation and more general expansions (see e.g. the discussion in Wei *et al.* 1995) may be in principle required. Such a high value for K has been considered owing to the small nonlinearities. Actually, for higher ϵ_p, increasing K would result in the steepening of the crests forming the dispersive tail until breaking occurs due to the interaction with the local disturbance.

4.2. *Supercritical regime*

Without entering into detail, we recall the major features of the supercritical regime. A typical result is considered in figure 6. It may be noted that the steady component of the wave pattern is now in the form of a hump, consistent with the weakly nonlinear description, see (3.10). The two unsteady signals, corresponding to the theoretically predicted f- and g-waves, are both left behind the forcing and, in particular, the g-type component, according to (3.8), has a negative mean value.

5. Transcritical regime

From the theory of §3 we know that, in transcritical conditions, $Fr \simeq 1$, the flow presents specific features. The pressure amplitude is now required to be of a lower

order ($O(\epsilon^2)$) than in the previous cases ($O(\epsilon)$), and a higher free-surface response to excitation ratio is obtained. Moreover, the range of validity with respect to the parameter $K^{-1} = \ell/L$, which measures the pressure extension in terms of the horizontal length scale, is now wider, including even very short base lengths. It is then possible to have water deep with respect to the disturbance length even though the flow regime corresponds to the long-wave limit.

According to the scalings given in §3.2, the proper set of dimensionless variables for the transcritical case ($i = 2$) is

$$x = \epsilon_p^{1/3}\frac{x^*}{h}, \qquad y = \frac{y^*}{h}, \qquad \tau = \epsilon_p \frac{t^*}{h/\mathscr{C}_0}, \qquad \eta = \epsilon_p^{-2/3}\frac{\eta^*}{h}, \qquad \mathscr{P} = \frac{p^*}{\epsilon_p \rho g h}, \tag{5.1}$$

which, although obtained through a different procedure, coincides exactly with those given in Akylas (1984). The corresponding wave forms scale according to

$$\eta^*(x^*, t^*) = h\epsilon_p^{2/3}\eta\left(\epsilon_p^{1/3}\frac{x^*}{h}, \epsilon_p \frac{t^*}{h/\mathscr{C}_0}\right). \tag{5.2}$$

For the present computations $h = 1$ and $K = 2.1542$, which, for $\epsilon_p = 0.1$, gives $\ell = 1.0$ (one of the cases considered in Wu 1987).

In the linear case, as discussed in Akylas (1984), the critical solution exhibits a divergent behaviour. Completely different wave patterns, discussed in Wu & Wu (1982) in the framework of the weakly nonlinear theory, are obtained when the nonlinear terms are retained. In particular the fully nonlinear results in figure 7 show a long-time behaviour characterized by the periodic emission of forward running waves. These periodic flow conditions define the transcritical regime, which in the context of a weakly nonlinear model, may be characterized more sharply, Shen (1993), in terms of a critical range for the detuning parameter $\lambda = \epsilon_p^{-2/3}(F - 1)$ centred around $\lambda = 0$ (see also the paper by Miles 1986).

Another distinguishing feature in figure 7 is the continuously developing region of depressed mean level, trailing the pressure disturbance. Further downstream, this almost flat portion is connected to the rightmost unperturbed free surface by a wavy transitional region (Wu 1987).

Figure 8 quantitatively compares the wave forms for two different amplitudes of the forcing. The fKdV model predicts the similarity of the solutions with respect to the forcing intensity ϵ_p, see (5.2). This result does not hold exactly in the present case, where the emitted wave heights, expressed in the variables (5.1), clearly show a dependence on the excitation amplitude. Consequently, as emerges from the figure, the phase speed is affected also. In this case the actual free-surface response is stronger than predicted by the fKdV model, a trend opposite to the one observed for the results given in §4. An extended comparison among the exact results and the weakly nonlinear models is presented in figure 9. The results of figure 10, which like the others shown in the present paper have been checked under time step and spatial grid refinement, report the wave pattern for several values of ϵ_p. In particular, when increasing the forcing, the steepening of the first crest trailing the disturbance is observed. Figure 11, for the specific value $\epsilon_p = 0.12$, shows the natural scale profile of the peaking crest.

The trailing wave system is discussed by considering, figure 12, a larger portion of the computational domain. Downstream of the depression, the mean water height gradually increases to the undisturbed level far from the disturbance. This intermediate region is characterized by a trailing system of waves whose amplitudes gradually decrease downstream (see e.g. the curve corresponding to $\tau = 7.5$). The

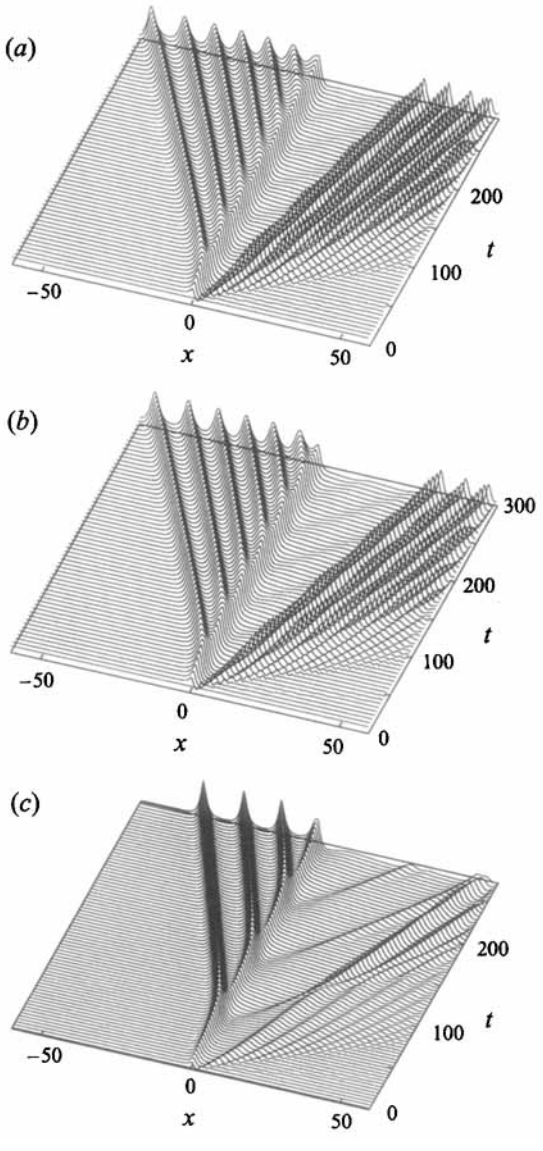

FIGURE 7. Nonlinear transcritical solutions ($\epsilon_p = 0.1$) following from the model of §2: (*a*) $Fr = 0.975$, (*b*) 1.0, (*c*) 1.1. The dimensionless variables are defined as in figure 2.

lengthening of the depressed region is accompanied by the development of the trailing system. A closer look (e.g. $\tau = 25$) reveals a modulation of the wave heights, which is related to small wave packets periodically emitted and propagating backwards through the depressed region (see also figure 7). Although not explicitly discussed there, this behaviour is also observed in the numerical solutions of the fKdV model, Wu (1987). In the reference frame of the disturbance, the waves are right propagating with a higher speed than the trailing system and, by interfering with the latter, originate the observed undulations.

The effect of the Froude number is considered in figure 13, where, for $\epsilon_p = 0.1$, three different configurations, corresponding to $\lambda < 0$, $\lambda = 0$ and $\lambda > 0$ respectively, are

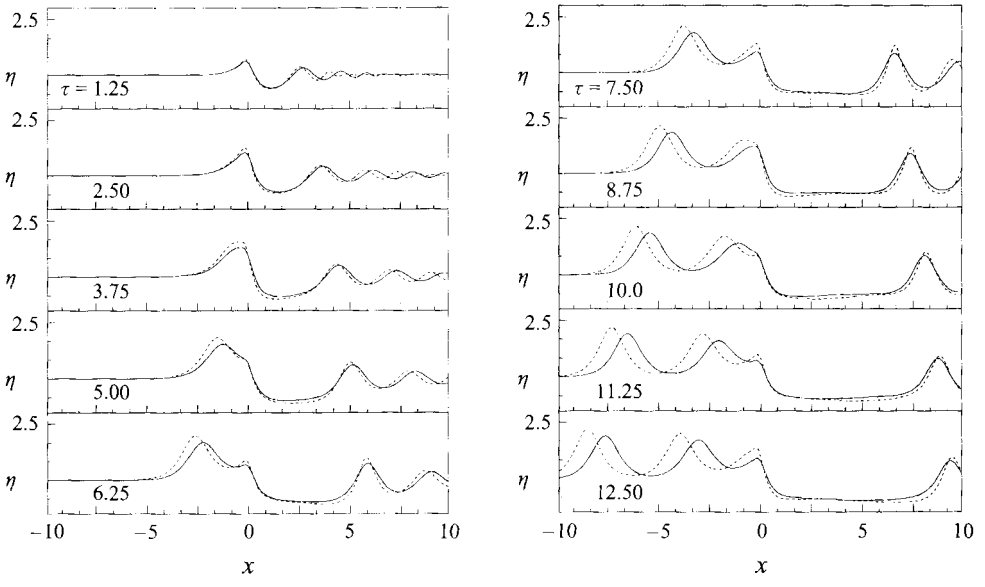

FIGURE 8. Fully nonlinear computations according to the formulation of §2. Wave forms for $\lambda = 0$ (critical conditions) for $\epsilon_p = 0.05$ (solid line) and $\epsilon_p = 0.1$ (broken line). Dimensionless variables according to (5.1).

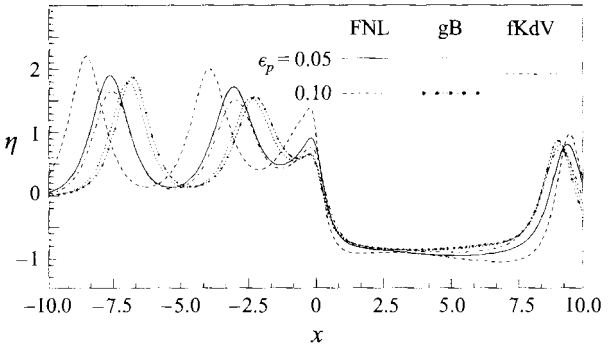

FIGURE 9. The wave patterns, predicted by the fully nonlinear model (FNL), the generalized Boussinesq system (gB) and the forced KdV equation (fKdV), are compared for the case of figure 8. $\tau = 12.5$, $\lambda = 0$.

reported for $\tau = 12.5$. The heights of the upstream waves increase with λ (figure 13*a*), since larger runaway velocities are required for increasing speed of the disturbance, thus implying higher waves. The opposite behaviour is observed in figure 13(*b*) for the trailing system, with higher crests for smaller values of λ. A larger subcritical detuning is considered in figure 14, where the upstream influence appears in the form of a developing undular bore, see e.g. Melville & Helfrich (1987). Despite the quantitative differences, the exact formulation and the weakly nonlinear models predict the same qualitative behaviour.

For sufficiently intense forcings, wave steepening is always observed and a consistent picture emerges from the simulations. Namely, for fixed ϵ_p, by decreasing λ, a region in the parameter space is entered where the breaking of the first trailing crest occurs, as already observed in figure 11. On the other hand, when λ is increased, the

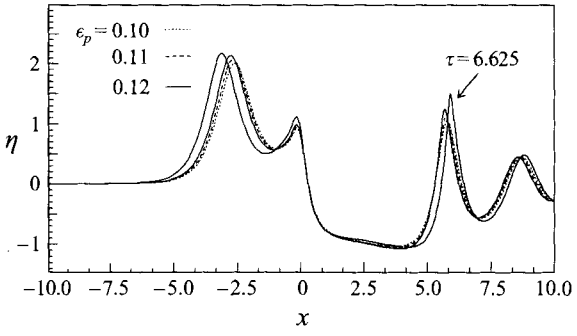

FIGURE 10. Wave patterns at the critical condition for high intensities of the forcing. $\tau = 6.25$, $\lambda = 0$. For $\epsilon_p = 0.12$ a later configuration shows the spilling behaviour of the first lee-wave crest.

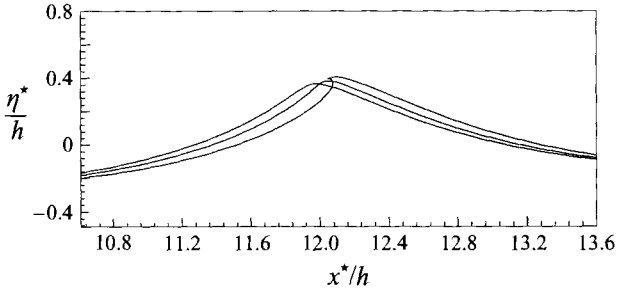

FIGURE 11. Steepening process for $\epsilon_p = 0.12$ in the natural scale. The three curves correspond to $\tau = 6.625$, 6.69 and 6.8, respectively.

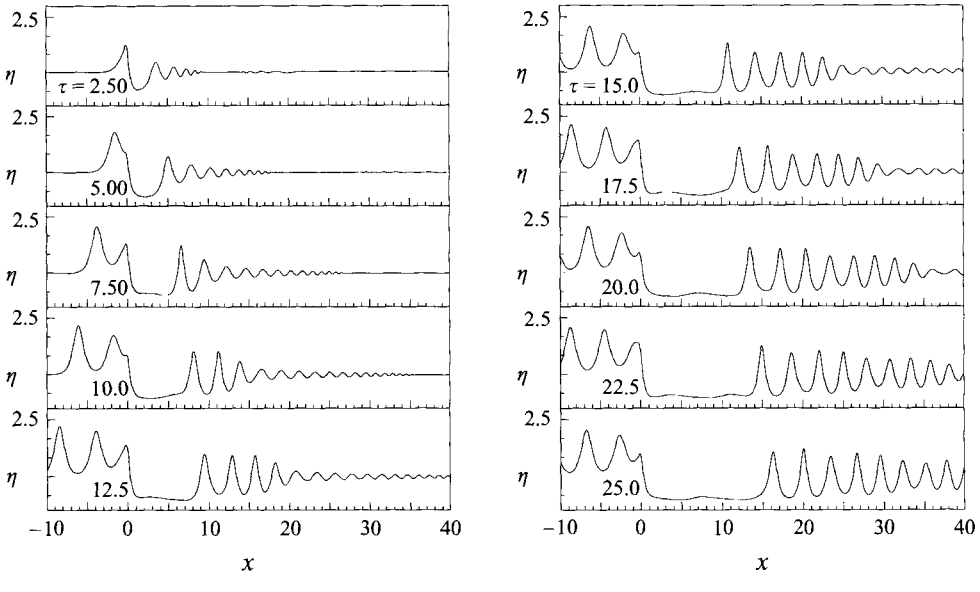

FIGURE 12. Long-time evolution of the free surface for $\epsilon_p = 0.1$ and $\lambda = 0$.

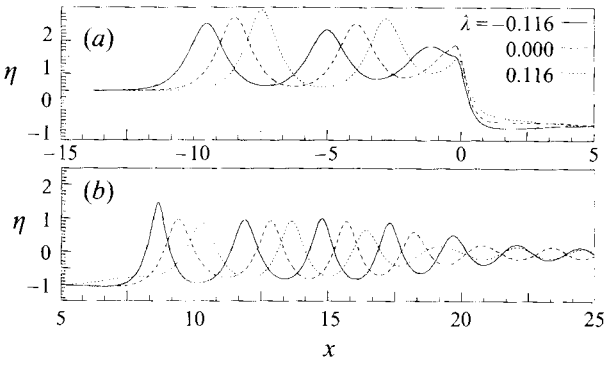

FIGURE 13. Effect of the detuning parameter λ on the wave pattern: (*a*) upstream-emitted and (*b*) trailing waves. $\tau = 12.5$, $\epsilon_p = 0.10$.

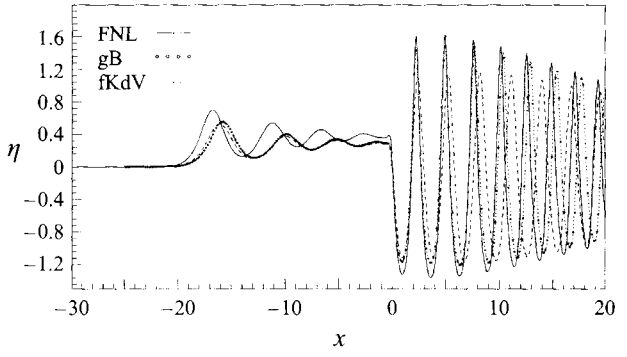

FIGURE 14. Development of the upstream undular bore for $\lambda = -0.928$, $\tau = 15.0$ and $\epsilon_p = 0.05$. The three curves report the fully nonlinear, the generalized Boussinesq and forced KdV wave patterns.

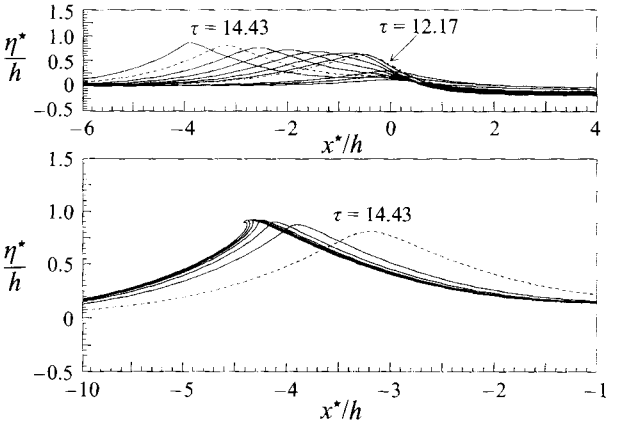

FIGURE 15. Growth and detachment of a forward running wave for a supercritical case (*a*): $Fr = 1.15$, $\lambda = 0.696$, $\epsilon_p = 0.1$; the time interval between wave profiles is $\Delta\tau \simeq 1.739$ for $\tau \leqslant 12.17$ (dash–dot line curve) and $\Delta\tau \simeq 0.348$ for $\tau \geqslant 12.17$. Soon after detachment, the packet loses its symmetry. The following evolution is reported in (*b*).

first upstream wave eventually undergoes localized steepening – see the natural scale profile in figure 15 – and finally overturns (figure 15*b*). This phenomenon, reported for the nominally two-dimensional experiments by Lee *et al.* (1989), is also observed in the three-dimensional transcritical flows about ship models by Ertekin *et al.* (1984). Although a systematic investigation has not been presently undertaken, critical conditions always separate the ranges of the two different behaviours. Additional results concerning wave breaking in transcritical flows are discussed in Teles da Silva & Peregrine (1992), where, instead of a pressure forcing, a moving bottom topography is considered.

The frequency of the emission corresponds to the time interval between two successive maxima in the wavemaking resistance. During the ripening phase the energy, supplied by the forcing, is stored in the nascent 'soliton' until a sufficient height is reached for detachment. Consistent with the weakly nonlinear results, Lee *et al.* (1989), the period increases with Froude number and decreases with the intensity of the forcing.

6. Concluding remarks

It is confirmed that weakly nonlinear models actually capture most of the features observed in the fully nonlinear solutions of forced long waves. Nevertheless, several points emerge from the present analysis. In particular, finite-amplitude effects are systematically observed in off-critical flows. Suitably designed numerical experiments, §4, enlightened the crucial role of the stage during which the f- and g-waves are generated. In fact, the KdV model assumes that the steady component and the emitted wave packets evolve with no interaction of one with the other. The physical interpretation of this hypothesis suggests the complete equivalence of the exact problem with the non-interacting evolutions for the f- and g-waves. This assumption may not be adequate during the generation, when the three waves are actually superimposed. The equivalence is found to hold in fact only for very weak forcings, as verified in detail. At higher amplitudes, the neglected interactions are responsible for the dependence of the solution, in terms of both amplitude and phase, on the forcing intensity, as correctly predicted by the gB model. For increasing dispersion, the agreement between the Boussinesq and the fully nonlinear description is lost. In these conditions the weakly nonlinear–weakly dispersive models require improvements in order to correctly predict the wave behaviour (Wei *et al.* 1995).

In subcritical conditions, the g-packet precedes the forcing and eventually splits into solitary-wave-like components, consistently with the weakly nonlinear descriptions.

The basic features provided by the weakly nonlinear theory are also confirmed for transcritical flows. However, we observed in this case the tendency toward wave breaking when the forcing exceeds a given threshold which is found to depend on the actual value of the detuning parameter. Furthermore, consistent with experimental observations, the breaking also tends to occur at the first trailing crest or at the first emitted soliton-like wave when the flow is slightly sub- or super-critical respectively.

The research of M.L. was partially supported by *Ministero dei Trasporti e della Navigazione* through INSEAN – Research Program 1994–96.

REFERENCES

AKYLAS, T. R. 1984 On the excitation of long nonlinear water waves by a moving pressure distribution. *J. Fluid Mech.* **141**, 455–466.

BAKER, G. R., MEIRON, D. I. & ORSZAG S. A. 1989 Generalized vortex methods for free surface flow problems. II: Radiating waves. *J. Sci. Comput.* **4**, 237–259.

BASSANINI, P., CASCIOLA, C. M., LANCIA, M. R. & PIVA, R. 1991 A boundary integral formulation for the kinetic field in aerodynamics. Part I. *Eur. J. Mech.* B/*Fluids* **10**, 605–627.

CASCIOLA, C. M. & PIVA, R. 1990 A boundary integral approach in primitive variables for free surface flows. In *Proc. 18th Symp. on Naval Hydrod.*, pp. 221–238. Washington D.C.: National Academy of Sciences.

COLE, S. L. 1985 Transient waves produced by flow past a bump. *Wave Motions* **7**, 579–587.

COOKER, M. J., PEREGRINE, D. H., VIDAL, C. & DOLD, D. J. 1990 The interaction between a solitary wave and a submerged semicircular cylinder. *J. Fluid Mech.* **215**, 1–22.

DOLD, J. W. 1992 An efficient surface integral algorithm applied to unsteady gravity waves. *J. Comput. Phys.* **103**, 90–115.

DOLD, J. W. & PEREGRINE, D. H. 1986 An efficient boundary integral method for steep unsteady water waves. In *Numerical Methods for Fluid Dynamics II* (ed. L. W. Morton and M. J. Baines), pp. 671–679. Oxford University Press.

DOMMERMUTH, D. G., YUE, D. K. P., RAPP, R. J., CHANN, E. S. & MELVILLE, W. K. 1988 Deep-water plunging breakers: a comparison between potential theory and experiments. *J. Fluid Mech.* **189**, 423–442.

ERTEKIN, R. C., WEBSTER, W. C. & WEHAUSEN, J. V. 1984 Ship generated solitons. In *Proc. 15th Symp. on Nav. Hydr.*, pp. 1–15. Washington DC: National Academy of Sciences.

FENTON, J. 1972 A ninth-order solution for the solitary wave. *J. Fluid Mech.* **53**, 257–271.

HUANG, D. D., SIBUL, O. J., WEBSTER, W. C., WEHAUSEN, J. V., WU, D. M. & WU, T.Y. 1982 In *Proc. Conf. on Behaviour of Ships in Restricted Waters*, vol. II, pp. 26.1–26.10. Varna: Bulgarian Ship Hydrodynamics Centre.

ISRAELI, M. & ORSZAG, S. 1981 Approximation of radiation boundary conditions. *J. Comput. Phys.* **41**, 115–135.

KEVORKIAN, J. & YU, J. 1989 Passage through the critical Froude number for shallow water waves over a variable bottom. *J. Fluid Mech.* **204**, 31–56.

LEE, S., YATES, G. T. & WU, T. 1989 Experiments and analyses of upstream-advancing solitary waves generated by moving disturbances. *J. Fluid Mech.* **199**, 569–593.

LONGUET-HIGGINS, M. S. & COKELET, E. D. 1976 The deformation of steep surface waves on water. I A numerical method of computation. *Proc. R. Soc. Lond.* A **350** 1–26.

MEI, C. C. 1989 *The Applied Dynamics of Ocean Surface Waves.* World Scientific.

MELVILLE, W. K. & HELFRICH, K. R. 1987 Transcritical two-layer flow over topography. *J. Fluid Mech.* **178**, 31–52.

MILES, J. W. 1986 Stationary, transcritical channel flow. *J. Fluid Mech.* **162**, 489–499.

NEW, A. L., MCIVER, P. & PEREGRINE, D. H. 1985 Computations of overturning waves *J. Fluid Mech.* **150**, 233–251.

ROBERTS, A. J. 1983 A stable and accurate numerical method to calculate the motion of a sharp interface between fluids. *IMA J. Appl. Maths* **31**, 13–35.

SEGUR, H. 1973 The Korteweg–de Vries equation and water waves. *J. Fluid. Mech.* **59**, 721–736.

SHEN, S. S. 1993 *A Course on Nonlinear Waves.* Kluwer.

SIDI, A. & ISRAELI, M. 1988 Quadrature methods for periodic singular and weakly singular fredholm integral equations. *J. Sci. Comput.* **3**, 201–231.

STOKER, J. J. 1957 *Water Waves.* Interscience.

TELES DA SILVA, A. F. & PEREGRINE, D. H. 1992 Wave breaking due to moving submerged obstacles. In *Proc. IUTAM Symp. on Wave Breaking, Sydney* (ed. Banner & Grimshaw), pp. 333–340. Springer.

THEWS, J. G. & LANDWEBER, L. 1936 *US Experimental Model Basin Rep.* 408–414. Washington DC: Navy Yard.

TOMASSON, G. G. & MELVILLE, W. K. 1991 Flow past a constriction in a channel: a modal description *J. Fluid Mech.* **232**, 21–45.

WEI, G., KIRBY, J. T., GRILLI, S. T. & SUBRAMANYA, R. 1995 A fully nonlinear Boussinesq model for surface waves. Part 1. highly nonlinear unsteady waves. *J. Fluid Mech.* **294**, 72–92.

VINJE, T. & BREVIG, P. 1981 Numerical simulations of breaking waves. In *Adv. Water Resources* **4**, 77–82.

WU, D. M. & WU, T. Y. 1982 Three-dimensional nonlinear long waves due to moving surface pressure. In *Proc. 14th Symp. on Nav. Hydr.*, pp. 103–125. Washington DC: National Academy of Sciences.

WU, T. Y. 1987 Generation of upstream solitons by moving disturbances. *J. Fluid Mech.* **184**, 75–99.